Electronic Supplementary Information (ESI) for

Electronic state modulation of Ag_{30} nanoclusters within a ring-shaped polyoxometalate

Daiki Yanai,[a] Kentaro Yonesato,*[a] Soichi Kikkawa,[b] Seiji Yamazoe,[b] Kazuya Yamaguchi,[a] and Kosuke Suzuki *[a]

[a] Department of Applied Chemistry, School of Engineering, The University of Tokyo, 7-3-1 Hongo, Bunkyo-ku, Tokyo 113-8656, Japan.

[b] Department of Chemistry, Graduate School of Science, Tokyo Metropolitan University, 1-1 Minami Osawa, Hachioji, Tokyo 192-0397, Japan.

Contents **Page**

Experimental section S2–S4
Table S1–S7 S5–S7
Fig. S1–S18 S8–S19
References S20

Experimental section

Instruments

Ultraviolet–visible absorption spectra were measured using a JASCO V-770 with a 1 cm quartz cell at room temperature (~25 °C). Infrared (IR) spectra were measured using a JASCO FT/IR-4100 with KBr pellets. Thermogravimetric and differential thermal analyses were performed using a Rigaku Thermo plus EVO2 TG-DTA8122 instrument. Inductively coupled plasma optical emission spectroscopy analyses for phosphorus, silver and tungsten were conducted using a Shimadzu ICPS-8100 spectrometer. Elemental analyses for carbon, hydrogen, and nitrogen were performed on a MICRO CORDER JM10 at the Materials Analysis Division, Open Facility center of Tokyo Institute of Technology. X-ray photoelectron spectroscopy (XPS) was performed using a JEOL JPS-9030 instrument. For curve fitting of the XPS spectra, the Shirley method was used for the background, and the fitting was performed with a Gauss–Lorentz type function.

Materials

N,*N*-dimethylformamide (DMF), ethyl acetate, acetonitrile, toluene, and *p*-toluenesulfonic acid monohydrate were purchased from Kanto Chemical. All solvents were dried using appropriate molecular sieves. Tetra-*n*-butylammonium hydroxide 30 hydrate, tetra-*n*-butylammonium borohydride ($TBABH_4$), and silver acetate were purchased from Sigma-Aldrich. Sodium trifluoromethanesulfonate was purchased from Alfa Aesar. $TBA_{12}H_{28}[P_8W_{48}O_{184}]\cdot 25H_2O$ and $TBA_{16}H_8[Ag_{16}(P_8W_{48}O_{184})]\cdot 12C_3H_6O\cdot 12H_2O$ (**Ag16**) and $TBA_{17}H[Ag_{30}(P_8W_{48}O_{184})]\cdot 10C_3H_7NO\cdot 30H_2O$ (**Ag30**), $TBA_{17}H_7[Ag_{16}(P_8W_{48}O_{184})]\cdot 15C_3H_7NO\cdot 22H_2O$ (**I**) were synthesized according to our previous reports.[S1]

Synthesis of $TBA_{17}H_5[Ag_{30}P_8W_{48}O_{184}]$ (II)

Silver acetate (26.7 mg, 0.16 mmol) and **Ag16** (180 mg, 10 μmol) was added to DMF (4.5 mL), and the solution was stirred for 10 min at room temperature (~25 °C). A DMF solution of $TBABH_4$ (500 μL, 20 μmol) was added dropwise into the solution, and the resulting solution was stirred for 3 days at room temperature (~25 °C). After the addition of ethyl acetate (20 mL), dark brown block crystals of **II** were obtained from the resulting solution. The brown block crystals suitable for X-ray crystallographic analysis were obtained by recrystallization from the mixture solvent of DMF and toluene. IR (KBr, cm^{-1}): 3445, 2959, 2936, 2874, 1631, 1486, 1466, 1383, 1138, 1085, 1014, 976, 924, 879, 810, 699, 575, 529, 476, 461, 422. Ultraviolet–visible absorption (acetonitrile): λ (ε) 472 nm ($7.54 \times 10^4\ M^{-1}\ cm^{-1}$). TG-DTA: weight loss 4.2 wt% at 180 °C. Elemental analysis: calcd. (%) for $TBA_{17}H_5[Ag_{30}P_8W_{48}O_{184}]\cdot 7C_3H_7NO\cdot 20H_2O$, C 17.37, H 3.51, N 1.66, P 1.22, Ag 15.98,W 43.59; found, C 17.08, H 3.40, N 1.72, P 1.19, Ag 15.58, W 44.10.

Reaction of II and $TBABH_4$

Compound **II** (10 mg) was dissolved in acetonitrile (1 mL), and an acetonitrile solution of $TBABH_4$ (50 μL, 0.5 equiv. with respect to **II**) was added dropwise into the solution. The resulting solution was stirred for 12 h at room temperature (~25 °C).

X-ray crystallographic analysis

Single-crystal X-ray diffraction measurement for **II** was performed on a BL02B1 beamline at the SPring-8 facility of the Japan Synchrotron Radiation Research Institute (Proposal number 2023B1842, 2023A1731) with a PILATUS3 X CdTe 1M detector at −173 °C. The incident X-ray beam was monochromatized by a Si(311) double-crystal monochromator (λ = 0.4132 Å). The data collection and process were conducted using RAPID AUTO and CrysAlisPro[S2] software, respectively. In the reduction of data, empirical, Lorentz and polarization corrections were made. The structural analysis was performed using WinGX.[S3] Structures were solved using SHELXT-2018/2 (intrinsic phase method)[S4] and refined by SHELXL-2018/3.[S5] All atoms were refined as anisotropic. The highly disordered TBA cations and solvent molecules were omitted by use of the SQUEEZE program.[S6] CCDC-2361048 contains the supplementary crystallographic data for **II**. These data can be obtained free of charge from The Cambridge Crystallographic Data Centre via www.ccdc.cam.ac.uk/data_request/cif.

Bond valance sum (BVS) calculation

The BVS values were calculated by the expression for the variation of the length r_{ij} of a bond between two atoms *i* and *j* in observed crystal with valence V_i.

$$V_i = \sum_j exp\left(\frac{r'_0 - r_{ij}}{B}\right)$$

where *B* is constant equal to 0.37 Å, r'_0 is bond valence parameter for a given atom pair.[S7]

Ag K-edge X-ray absorption fine structure (XAFS) measurements

Ag K-edge XAFS measurements were performed at beamline BL01B1 at the SPring-8 facility of the Japan Synchrotron Radiation Research Institute (Proposal number 2023B1651, 2023B2070). The incident X-ray beam was monochromatized by a Si(311) double-crystal monochromator. Solid-state XAFS measurements were conducted in transmission mode at −263 °C using a cryostat with liquid helium. Solution-state XAFS measurements were conducted on the solution of **II** (1 mM acetonitrile solution, 1 cm cell) with addition of TsOH (0.1 mM acetonitrile solution) at room temperature (~ 25 °C) and recorded in transmission mode using ionization chambers. XANES and EXAFS spectra were analyzed using the xTunes program.[S8] XANES spectra were obtained after normalization. Pre-edge background and EXAFS background were subtracted using McMaster and Cubicspline methods, respectively. EXAFS spectra were also obtained as k^3-weighted χ spectra after normalization. Fitting analysis for Fourier-transformed EXAFS spectra was conducted using the FEFF8 program.[S9]

Computational calculations

All calculations were performed with Gaussian 16 revision B.01. We performed the DFT calculations using CAM-B3LYP functional, and the solvent effects were included using the polarizable continuum model (PCM, acetonitrile). We employed the moderate-size basis set (6-31G* for O and P, 6-31G for H, and LANL2DZ ECP for W and Ag) because the size of the target molecule is large. The geometries of Ag, P, O, and W atoms determined by the crystallographic analysis of **II** were used in the DFT calculations. Protons on **P8W48** were positioned by the following protocol: the BVS calculations showed the lower BVS values of 16 oxygen atoms inside **P8W48** (O1–O16, 1.32–1.47, Figure S16a) than other oxygen atoms (1.52–2.20), indicating that these oxygen atoms are more basic and easily protonated. Therefore, taking into account structural symmetry and natural charge order obtained by DFT calculations, 4, 8, and 12 protons were added on these oxygen atoms (O1–O12) of **II** (Figure S16b).

Table S1. X-ray crystallographic parameters for **II**.

Crystal system	Tetragonal
Space group	*I*4/*m* (#87)
a (Å)	32.2143(3)
b (Å)	32.2143(3)
c (Å)	27.1465(4)
α (deg)	90
β (deg)	90
γ (deg)	90
V (Å^3)	28171.6(7)
Z	2
ρ_{calc} (g cm^{-3})	1.798
Temp. (K)	100(2)
R_1	0.0668
wR_2	0.2497
GOF	1.040

Table S2. Ag···Ag separations (Å) within $\{Ag_{30}\}^{18+}$ nanocluster of **II**.

Ag1	…	Ag1	3.091(6)	Ag2A	…	Ag5A	2.687(4)	Ag2A	…	Ag6B	2.817(5)
Ag1	…	Ag3	2.913(4)	Ag2A	…	Ag7A	2.776(5)	Ag2A	…	Ag8B	2.812(7)
Ag1	…	Ag4	3.084(4)	Ag2B	…	Ag6A	2.758(4)	Ag2B	…	Ag5B	2.707(6)
Ag2A	…	Ag2A	2.815(5)	Ag2B	…	Ag8A	2.800(4)	Ag2B	…	Ag7B	2.744(6)
Ag2A	…	Ag3	2.830(3)	Ag3	…	Ag5A	2.875(5)	Ag3	…	Ag5B	2.908(9)
Ag2A	…	Ag4	2.885(3)	Ag3	…	Ag6A	2.838(7)	Ag3	…	Ag6B	2.840(9)
Ag2B	…	Ag2B	2.813(4)	Ag4	…	Ag6A	2.872(7)	Ag4	…	Ag6B	2.90(1)
Ag2B	…	Ag3	2.881(3)	Ag4	…	Ag7A	2.811(8)	Ag4	…	Ag7B	2.72(1)
Ag2B	…	Ag4	2.880(3)	Ag5A	…	Ag6A	2.888(7)	Ag5B	…	Ag6B	2.84(1)
Ag3	…	Ag4	2.756(3)	Ag5A	…	Ag6A	2.978(7)	Ag5B	…	Ag6B	2.93(1)
				Ag5A	…	Ag7A	2.822(4)	Ag5B	…	Ag7B	2.838(6)
				Ag6A	…	Ag6A	2.877(7)	Ag6B	…	Ag6B	2.799(9)
				Ag6A	…	Ag6A	2.879(7)	Ag6B	…	Ag6B	2.87(1)
				Ag6A	…	Ag7A	2.830(8)	Ag6B	…	Ag7B	2.83(1)
				Ag6A	…	Ag7A	2.855(7)	Ag6B	…	Ag7B	2.77(1)
				Ag6A	…	Ag8A	2.809(9)	Ag6B	…	Ag8B	2.85(1)
				Ag7A	…	Ag8A	2.793(9)	Ag7B	…	Ag8B	2.91(1)

Table S3. Ag···Ag separations (Å) within $\{Ag_{30}\}^{16+}$ nanocluster of **I**.

Ag1	…	Ag1	3.114(6)	Ag2A	…	Ag5A	2.721(8)	Ag2A	…	Ag6B	2.80(2)
Ag1	…	Ag3	2.884(6)	Ag2A	…	Ag7A	2.77(1)	Ag2A	…	Ag8B	2.78(1)
Ag1	…	Ag4	3.057(5)	Ag2B	…	Ag6A	2.75(2)	Ag2B	…	Ag5B	2.65(1)
Ag2A	…	Ag2A	2.818(7)	Ag2B	…	Ag8A	2.768(8)	Ag2B	…	Ag7B	2.76(2)
Ag2A	…	Ag3	2.848(5)	Ag3	…	Ag5A	2.888(9)	Ag3	…	Ag5B	2.90(1)
Ag2A	…	Ag4	2.882(5)	Ag3	…	Ag6A	2.83(2)	Ag3	…	Ag6B	2.78(2)
Ag2B	…	Ag2B	2.820(7)	Ag4	…	Ag6A	2.82(1)	Ag4	…	Ag6B	2.91(2)
Ag2B	…	Ag3	2.893(5)	Ag4	…	Ag7A	2.80(1)	Ag4	…	Ag7B	2.81(2)
Ag2B	…	Ag4	2.898(5)	Ag5A	…	Ag6A	2.88(1)	Ag5B	…	Ag6B	2.91(2)
Ag3	…	Ag4	2.777(4)	Ag5A	…	Ag6A	2.93(2)	Ag5B	…	Ag6B	2.96(2)
				Ag5A	…	Ag7A	2.816(6)	Ag5B	…	Ag7B	2.88(1)
				Ag6A	…	Ag6A	2.88(3)	Ag6B	…	Ag6B	2.81(5)
				Ag6A	…	Ag6A	2.80(4)	Ag6B	…	Ag6B	3.06(5)
				Ag6A	…	Ag7A	2.83(2)	Ag6B	…	Ag7B	2.87(2)
				Ag6A	…	Ag7A	2.80(2)	Ag6B	…	Ag7B	2.86(2)
				Ag6A	…	Ag8A	2.82(2)	Ag6B	…	Ag8B	2.92(2)
				Ag7A	…	Ag8A	2.81(1)	Ag7B	…	Ag8B	2.85(2)

Table S4. BVS values for P and W atoms of **II**.

P1A	4.60	P2A	5.13		
P1B	4.97	P2B	5.13		
W1A	6.01	W2A	6.21	W3A	5.90
W4A	5.90	W5A	5.99	W6A	6.11
W1B	6.11	W2B	6.20	W3B	5.83
W4B	6.08	W5B	6.00	W6B	6.08

Table S5. Result of curve fitting analysis of Ag 3d XPS spectrum of **II**.

	Region	Binding energy (eV)	FWHM (eV)	Gauss (%)	Area (%)
Ag^0	$3d_{5/2}$	367.9	0.79	70	23
	$3d_{3/2}$	373.9			17
Ag^+	$3d_{5/2}$	367.5			35
	$3d_{3/2}$	373.5			25

Table S6. Fitting parameters on solid-state Ag K-edge EXAFS of **II** and **I** measured at −263°C.[a]

	Bond	CN[b]	*R* (Å)	Δ*E* (eV)	$(DW^c)^2$ ($Å^2$)	*R* factor (%)
II	Ag–Ag	4.9(3)	2.81(3)	2.3(5)	$9(3) \times 10^{-3}$	8.8
I	Ag–Ag	3.9(3)	2.77(3)	−1.3(5)	$9(5) \times 10^{-3}$	8.5
Ag foil[d]	Ag–Ag	10.4(3)	2.86(2)	2.1(3)	$1.0(3) \times 10^{-2}$	5.1

[a] *R* range; 2.0–3.0 Å, back *k* range; 3–16 $Å^{-1}$. The corresponding spectra were displayed in Fig. 3c (*k*-space) and Fig. 3d (Fourier-transformed *R*-space). [b] Coordination number. [c] Debye-Waller factor. [d] Measured at room temperature (~ 25 °C).

Table S7. The natural charge population of $\{Ag_{30}\}^{18+}$ nanocluster within a ring-shaped POM with $4H^+$ (i.e., $[H_4P_8W_{48}O_{184}]^{36-}$) on the natural charge population analysis.

Ag1	0.578	Ag2A	0.458	Ag2B	0.544
Ag3	0.682	Ag4	−0.331	Ag5	0.808
Ag6	−0.155	Ag7	−0.531	Ag8	0.669

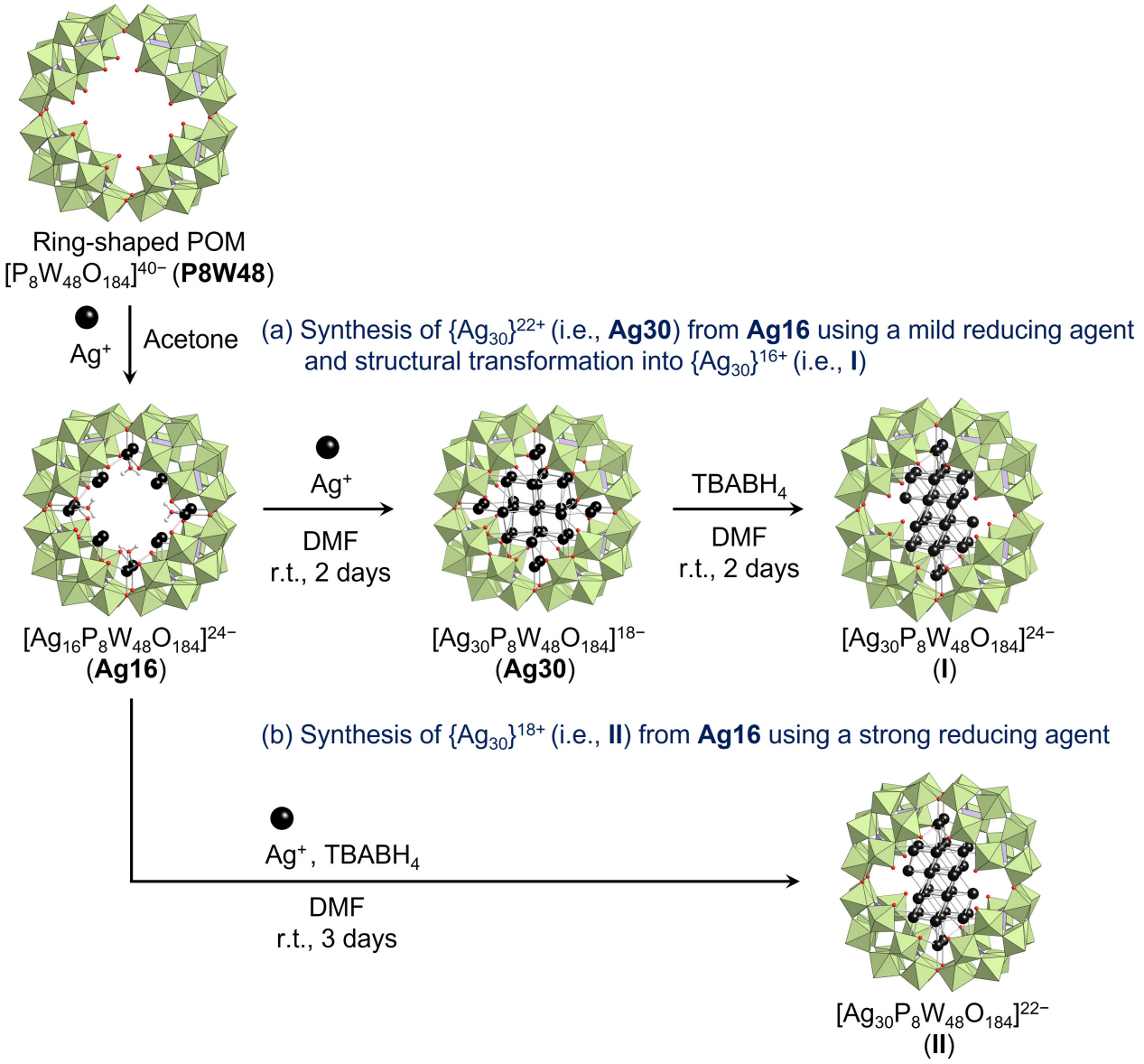

Fig. S1 Schematic for the synthesis of (a) $\{Ag_{30}\}^{16+}$ (i.e., **I**) and (b) $\{Ag_{30}\}^{18+}$ (i.e., **II**) nanocluster within the ring-shaped POM. Green octahedra, $\{WO_6\}$; purple tetrahedra, $\{PO_4\}$; black spheres, Ag atoms; red spheres, O atoms.

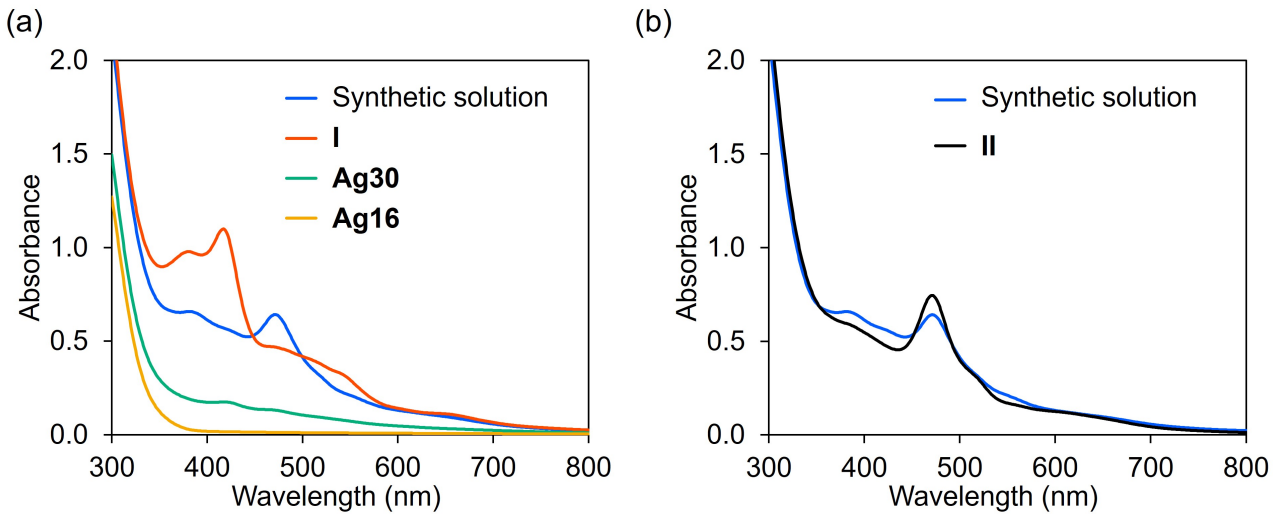

Fig. S2 (a) UV-vis spectra of the synthetic solution of **II** after 3 days (diluted with acetonitrile; blue line), **I** (red line), **Ag30** (green line), and **Ag16** (orange line) in acetonitrile ([POM] = 10 μM). (b) UV-vis spectra of the synthetic solution of **II** after 3 days (diluted with acetonitrile; blue line) and **II** (black line) in acetonitrile ([POM] = 10 μM).

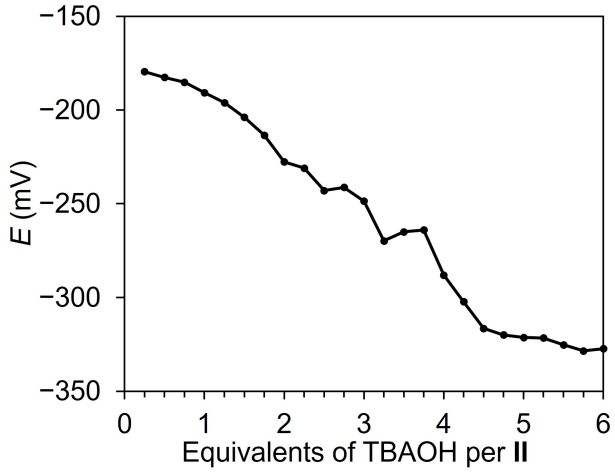

Fig. S3 Acid-base titration curve for **II** using TBAOH (15 mM) as a titrant in acetonitrile.

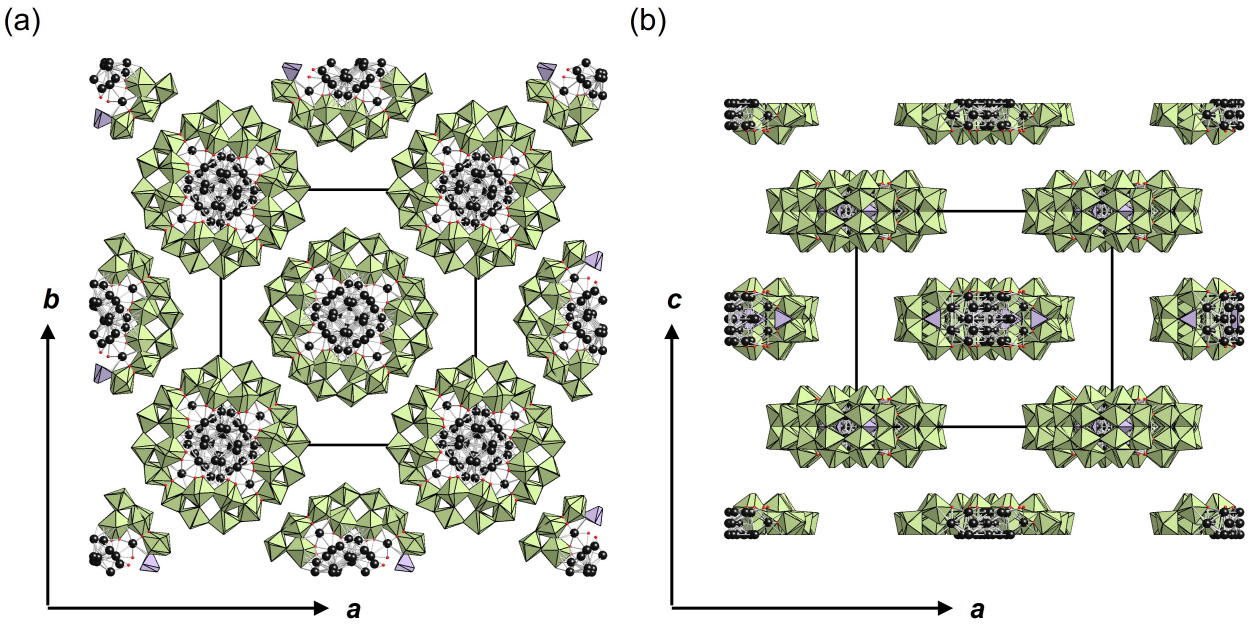

Fig. S4 Packing of **II** based on the X-ray crystallographic analysis in polyhedral model. (a) Views from the *c*-axis direction. (b) Views from the *b*-axis direction.

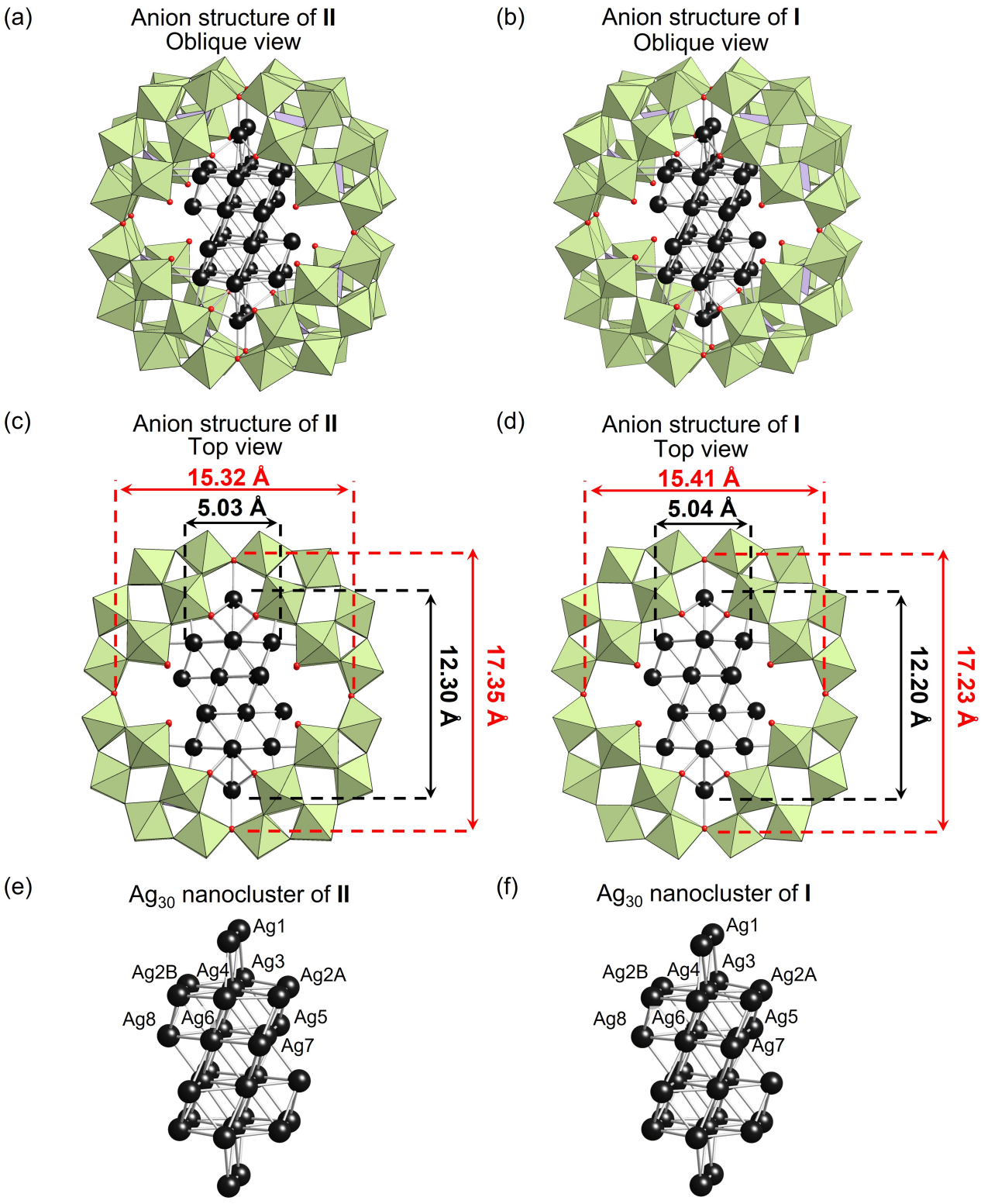

Fig. S5 Crystal structures depicting anion parts of **II** and **I**. Oblique views of anion parts of (a) **II** and (b) **I**. Top views of the anion parts of (c) **II** and (d) **I**. Structures of Ag_{30} nanoclusters in (e) **II** and (f) **I**. Green octahedra, $\{WO_6\}$; purple tetrahedra, $\{PO_4\}$; black spheres, Ag atoms; red spheres, O atoms.

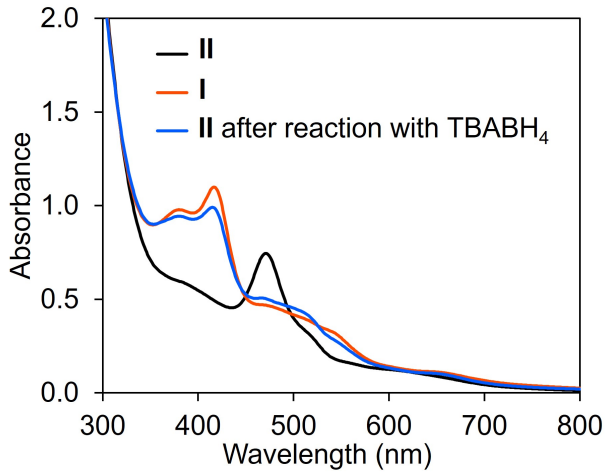

Fig. S6 UV-vis spectra of **I** and **II** in acetonitrile, and the reaction solution of **II** (10 μM) and $TBABH_4$ (0.5 equiv. with respect to **II**) in acetonitrile at room temperature (~25 °C) for 12 h.

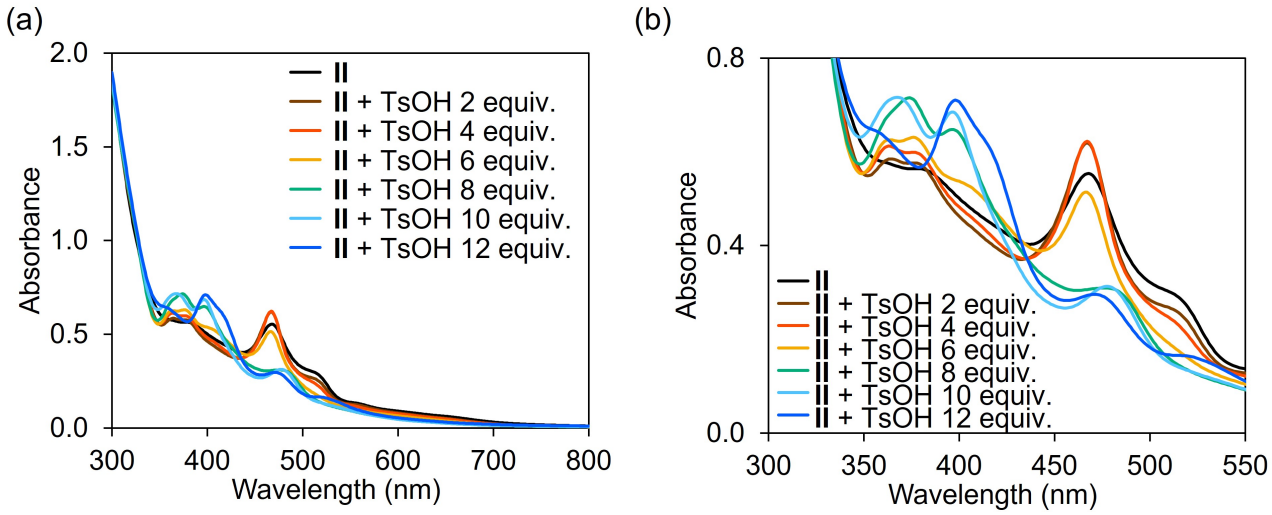

Fig. S7 (a) Wide view and (b) enlarged view of the UV-vis spectra of **II** with addition of TsOH in acetonitrile.

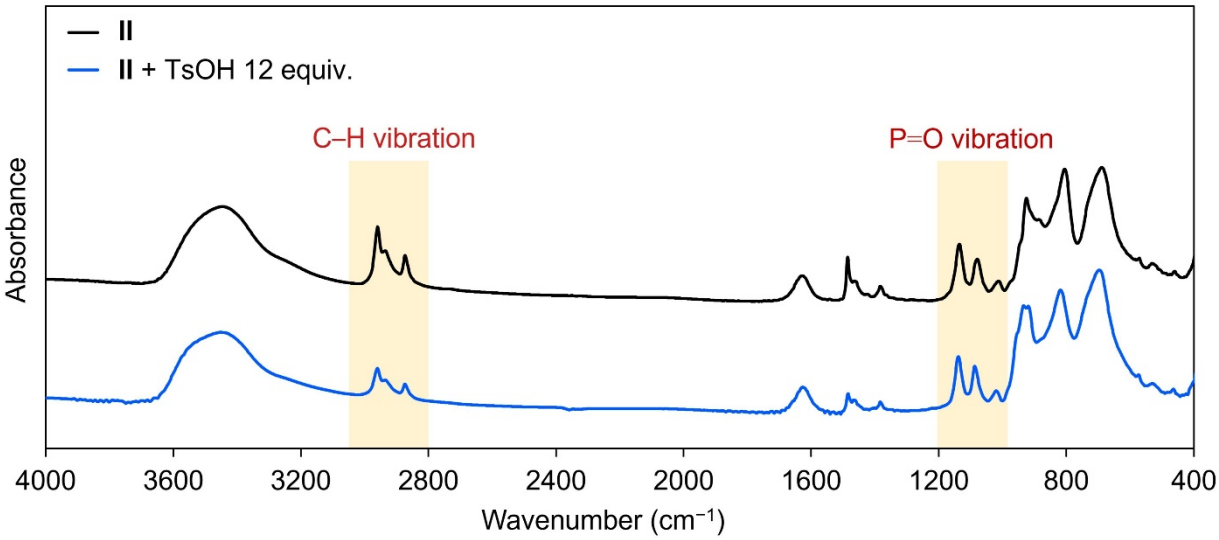

Fig. S8 IR spectra of **II** (black line) and **II** after the reaction with TsOH (12 equiv. with respect to **II**; blue line) (KBr pellet).

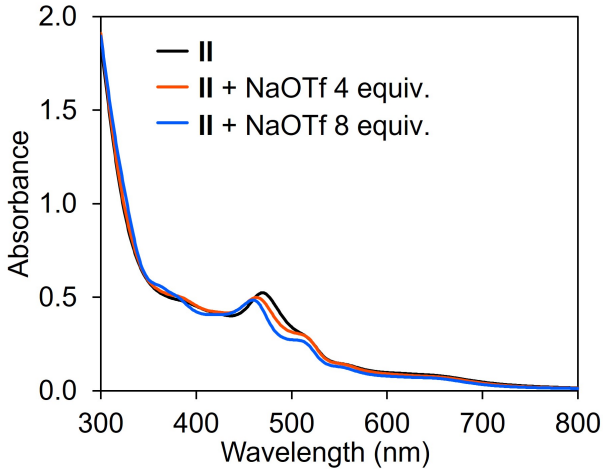

Fig. S9 UV-vis spectra of **II** with addition of sodium trifluoromethanesulfonate (NaOTf) in acetonitrile.

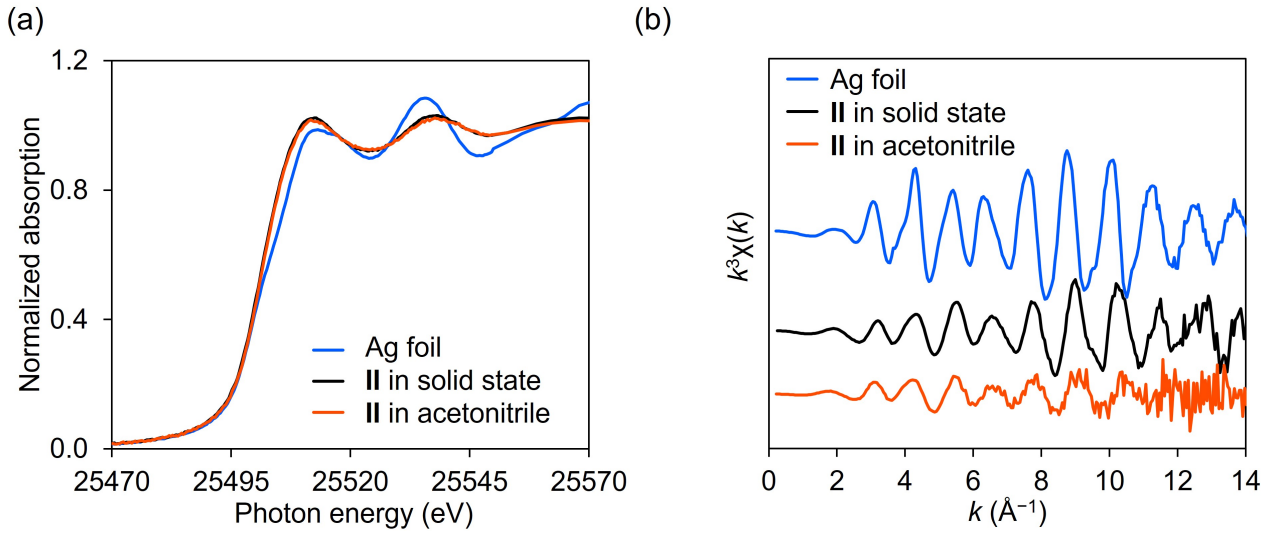

Fig. S10 Ag K-edge (a) XANES and (b) *k*-space EXAFS spectra of Ag foil (measured at ~25°C; blue line), **II** in solid state (measured at −263°C; black line), and **II** in acetonitrile (1 mM, measured at ~25°C; red line).

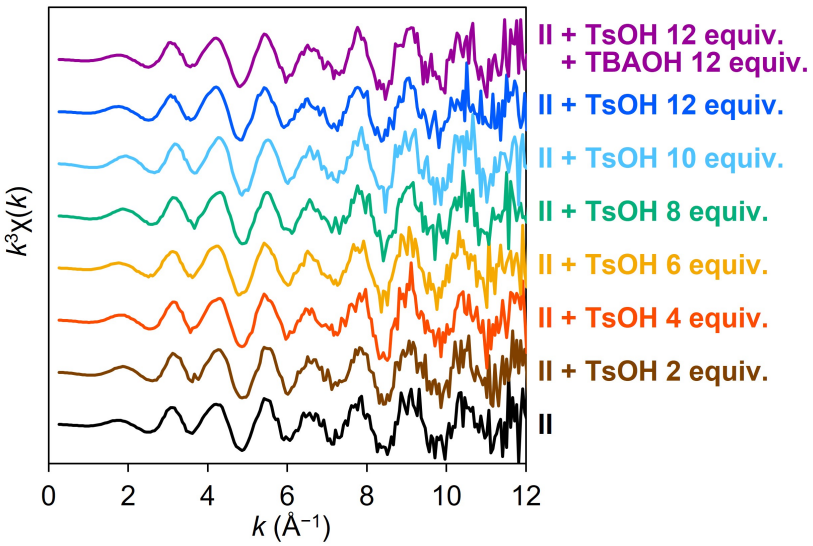

Fig. S11 Solution-state Ag K-edge k^3-weighted k-space EXAFS spectra of **II** upon addition of TsOH and TBAOH in acetonitrile.

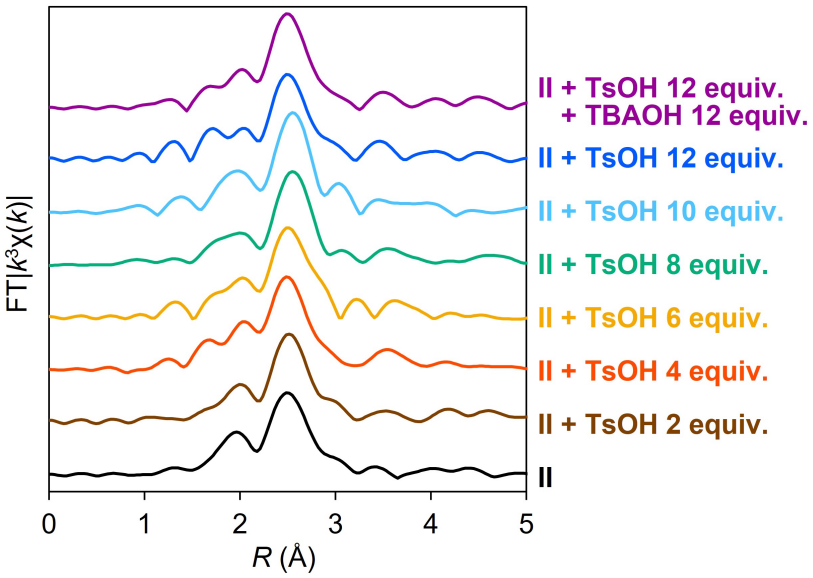

Fig. S12 Solution-state Ag K-edge Fourier-transformed R-space EXAFS spectra of **II** upon addition of TsOH and TBAOH in acetonitrile (k = 3–14 Å^{-1}).

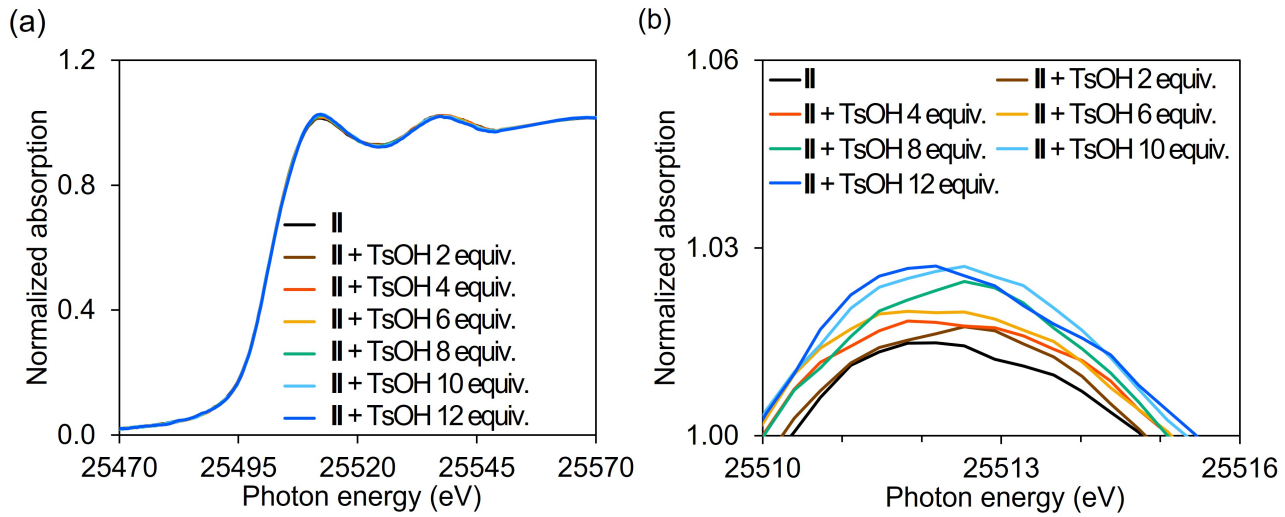

Fig. S13 (a) Wide view and (b) enlarged view of solution-state Ag K-edge XANES spectra of **II** with addition of TsOH in acetonitrile.

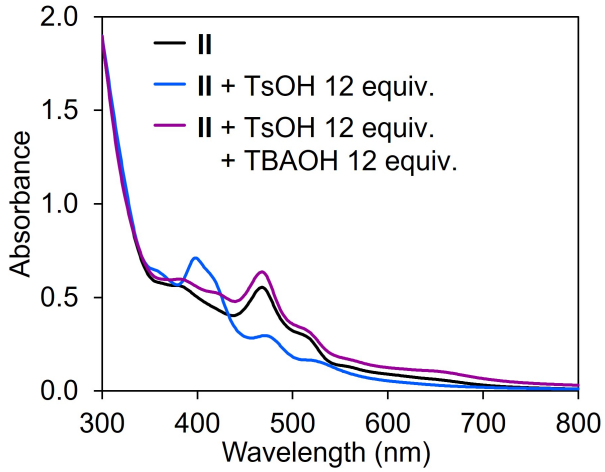

Fig. S14 UV-vis spectra of **II** (black line), **II** after addition of TsOH (12 equiv. with respect to **II**; blue line), and **II** after addition of TsOH and TBAOH (12 equiv. with respect to **II**; purple line) in acetonitrile.

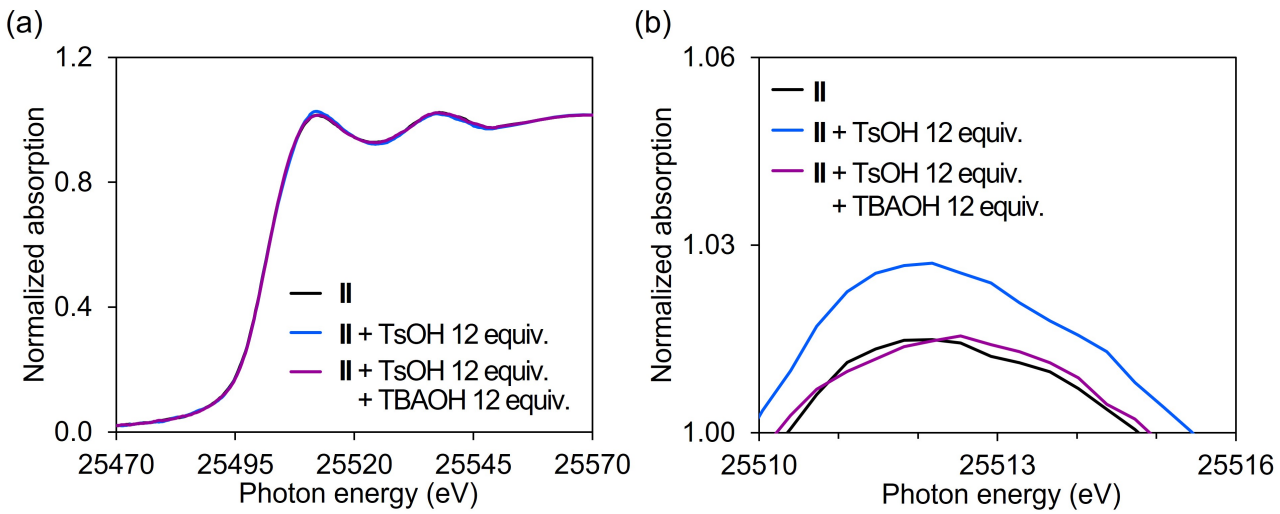

Fig. S15 (a) Wide view and (b) enlarged view of solution-state Ag K-edge XANES spectra of **II** (black line), **II** after addition of TsOH (12 equiv. with respect to **II**; blue line), and **II** after addition of TsOH and TBAOH (12 equiv. with respect to **II**; purple line) in acetonitrile.

(a)

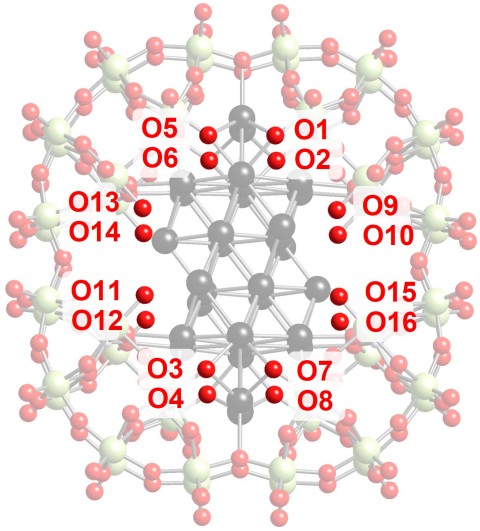

	Natural charge
O1 – O4	−0.80
O5 – O8	−0.78
O9 – O12	−0.77
O13 – O16	−0.71

(b)

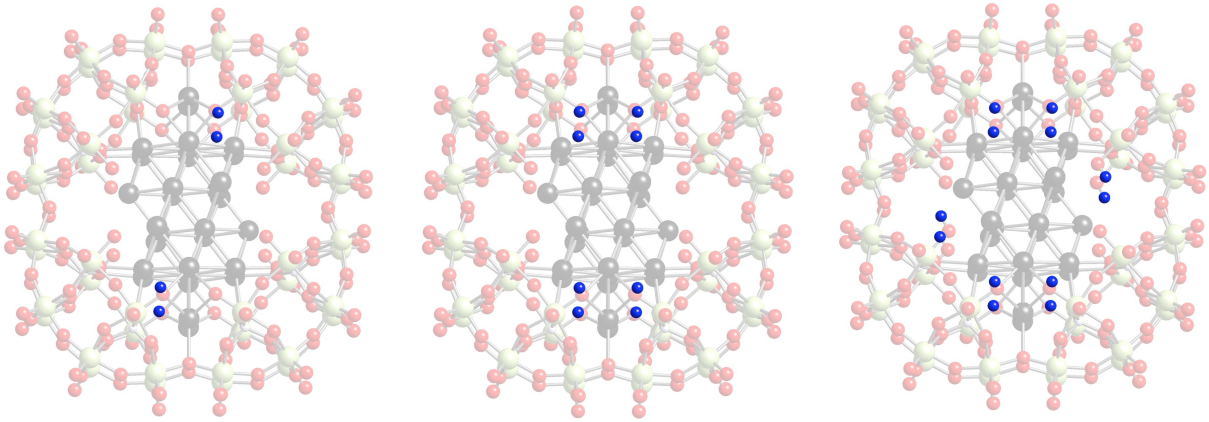

$[H_4P_8W_{48}O_{184}]^{36-}$ $[H_8P_8W_{48}O_{184}]^{32-}$ $[H_{12}P_8W_{48}O_{184}]^{28-}$

Fig. S16 (a) Schematic of the natural charge population of 16 basic oxygen atoms of the $[P_8W_{48}O_{184}]^{40-}$ ligand of the $\{Ag_{30}\}^{18+}$ nanocluster (i.e., **II**) based on the DFT study. (b) The geometries used in the DFT studies on the $\{Ag_{30}\}^{18+}$ nanoclusters within $[P_8W_{48}O_{184}]^{40-}$ with addition of 4, 8, and 12 protons. Green spheres, W atoms; purple spheres, P atoms; black spheres, Ag atoms; red spheres, O atoms; blue spheres, H atoms.

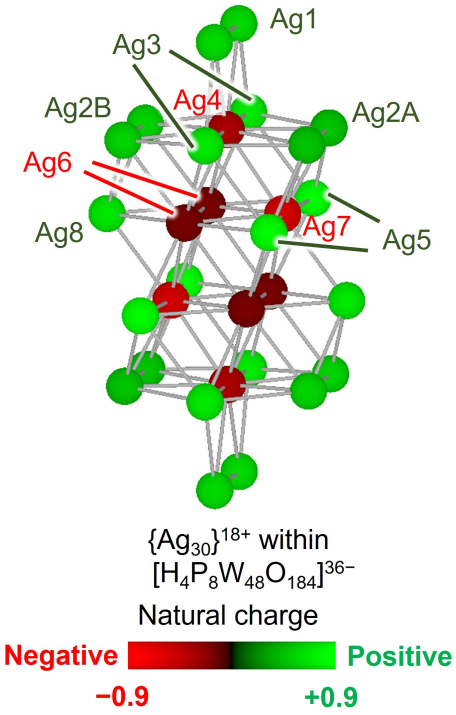

Fig. S17 Schematic of the natural charge population of the $\{Ag_{30}\}^{18+}$ nanocluster within a ring-shaped POM ($[H_4P_8W_{48}O_{184}]^{36-}$) based on the DFT study. Ag atoms with positive natural charge (0.46 – 0.81) and those with negative natural charges (−0.33 – −0.16) were displayed as green spheres and red spheres, respectively.

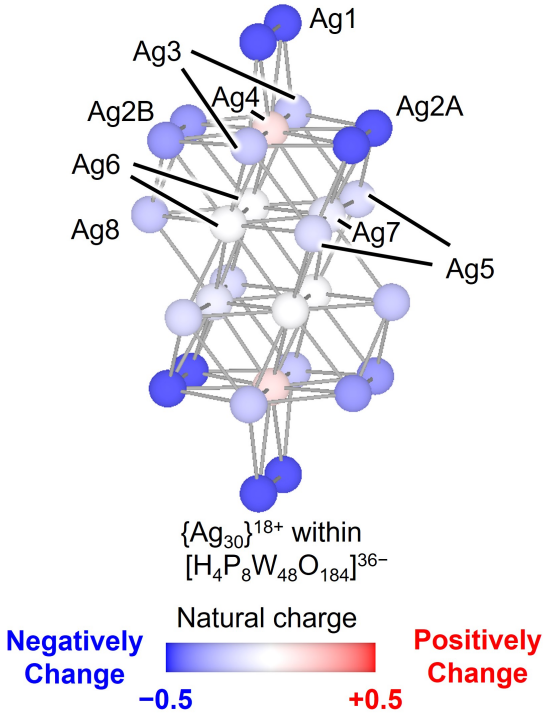

Fig. S18 Schematic of the natural charge changes of the $\{Ag_{30}\}$ nanocluster with a ring-shaped POM $[H_4P_8W_{48}O_{184}]^{36-}$ compared with the $\{Ag_{30}\}$ nanocluster without the ring-shaped POM. Ag atoms are colored according to the changes in the natural charges.

References

S1 (*a*) S. Sasaki, K. Yonesato, N. Mizuno, K. Yamaguchi and K. Suzuki, *Inorg. Chem.*, 2019, **58**, 7722–7729; (*b*) K. Yonesato, D. Yanai, S. Yamazoe, D. Yokogawa, T. Kikuchi, K. Yamaguchi and K. Suzuki, *Nat. Chem.*, 2023, **15**, 940–947.

S2 Rigaku OD. CrysAlis PRO. Rigaku Oxford Diffraction Ltd and Yarnton, England (2018).

S3 L. J. Farrugia, *J. Appl. Cryst.*, 2012, **45**, 849–854.

S4 G. M. Sheldrick, *Acta Crystallogr. A*, 2015, **71**, 3–8.

S5 (*a*) G. M. Sheldrick, *Acta Crystallogr. A*, 2008, **64**, 112–122; (*b*) G. M. Sheldrick, *Acta Crystallogr. C*, 2015, **71**, 3–8.

S6 P. van der Sluis and A. L. Spek, *Acta Crystallogr. A*, 1990, **46**, 194–201.

S7 N. E. Brese and M. O'Keeffe, *Acta Crystallogr. B*, 1991, **47**, 192–197.

S8 H. Asakura, S. Yamazoe, T. Misumi, A. Fujita, T. Tsukuda and T. Tanaka, *Radiat. Phys. Chem.*, 2020, **175**, 108270.

S9 A. L. Ankudinov, B. Ravel, J. J. Rehr and S. D. Conradson, *Phys. Rev. B*, 1998, **58**, 7565–7576.